HHS Public Access

Author manuscript

*Sens Actuators B Chem*. Author manuscript; available in PMC 2015 December 15.

Published in final edited form as:

*Sens Actuators B Chem*. 2014 December 15; 205: 313–321. doi:10.1016/j.snb.2014.08.073.

# Detecting De-gelation through Tissue Using Magnetically Modulated Optical Nanoprobes (MagMOONs)

**KhanhVan T. Nguyen** and **Jeffrey N. Anker***

Department of Chemistry, Center for Optical Materials Science and Engineering Technology (COMSET), SC BioCRAFT and Environmental Toxicology Program, Clemson University, Clemson SC 29634

## Abstract

Alginate gels are widely used for drug delivery and implanted devices. The rate at which these gels break down is important for controlling drug release. Since the de-gelation may be different *in vivo*, monitoring this process *in situ* is essential. However, it is challenging to monitor the gel through tissue due to optical scattering and tissue autofluorescence. Herein we describe a method to detect through tissue the chemically-induced changes in viscosity and de-gelation process of alginate gels using magnetically modulated optical nanoprobes (MagMOONs). The MagMOONs are fluorescent magnetic microspheres coated with a thin layer of opaque metal on one hemisphere. The metal layer prevents excitation and emission light from passing through one side of the MagMOONs, which creates orientation-dependent fluorescence intensity. The magnetic particles also align in an external magnetic field and give blinking signals when they rotate to follow an external modulated magnetic field. The blinking signals from these MagMOONs are distinguished from background autofluorescence and can be tracked on a single particle level in the absence of tissue, or for an ensemble average of particles blinking through tissue. When these MagMOONs are dispersed in calcium alginate gel, they become sensors for detecting gel degradation upon addition of either ammonium ion or alginate lyase. Our results show MagMOONs start blinking approximately 10 minutes after 2 mg/mL alginate lyase addition and this blinking is clearly detected even through up to 4 mm chicken breast. This approach can potentially be employed to detect bacterial biofilm formation on medical implants by sensing specific proteases that either activate a related function or regulate biofilm formation. It can also be applied to other biosensors and drug delivery systems based on enzyme-catalyzed breakdown of gel components.

### Keywords

MagMOONs; fluorescence; alginate lyase; tissue; de-gelation

* **janker@clemson.edu**.



Appendix A. Supplementary data

Supplementary data showing additional figures is available online.

## 1. Introduction

Alginate gels and their derivations are widely used for implanted devices and drug delivery [1-3]. These gels can serve as local source of proteins, nucleic acids, and small molecule drugs; and the degradation of the gels will release them [4-8]. The gels are also used in wound dressings and as a platform for cell culture [9, 10]. They are increasingly used in tissue regeneration by carrying and delivering proteins and cells that promote bone, muscle, cartilage and blood vessels formation [11-14].

In general, a gel allows small molecules and particles to diffuse through it, but effectively prevents the motion of particles that are large compared to the gel network mesh size. The gel can be dissolved by either breaking the crosslinks in the gel network, or enzymatically cleaving the polymer backbones allowing rapid drug release. After the gel breaks down, larger probes become free to move and the effective viscosity dramatically decreases. Detecting this rapid change in viscosity during de-gelation can also be used to determine the activity of enzymes that digest the gel. *In vitro* viscosity can be measured using standard viscometers such as capillary [15], plate, or falling ball viscometers [16]. To measure local viscosity in confined systems such as a cellular cytoplasm or measurement through tissue, more sophisticated methods are needed to apply force to a probe and measure its response. Möller and colleagues measured the local viscoelastic moduli of the macrophages cytoplasm by recording the deflection and recovery of 1.3 μm magnetic beads when applying twisting force pulses [17]. They also studied the intracellular phagosome transport in macrophages by monitoring the remnant magnetic field of ~ $10^6$ phagocytized magnetic particles after initially magnetizing them with a strong magnetic field. The remnant magnetic field decayed as each particle rotated away from its initial orientation by independent intracellular transport forces in each cell [18]. This is an excellent non-invasive approach for intracellular investigation. However, they required $10^6$ particles to measure the remnant magnetic field and the approach cannot take advantage of the single particle tracking to obtain local information of the surrounding of each individual particle using this method. In addition to magnetometry approaches, mechanical methods based on oscillation or vibration of a cantilever have also been developed [19, 20]. For example, Ehrlich and co-workers designed a wireless biosensor device for early biofilm detection based on changes in the resonance frequency of a cantilever in response to change in viscosity as a polysaccharide gel was cleaved by its enzyme galactosidase [19]. This galactosidase enzyme was designed to activate upon binding of RAP (Ribonucleic acid [RNA] III activating protein), a quorum sensing molecule generated by bacteria. When activated by RAP, the enzyme cleaved a polysaccharide substrate and produced glucose, which broke down a dextran-Concanavalin A hydrogel by competing with the dextran for binding to the Concanavalin A crosslinks. This RAP-activated gel breakdown reduced the hydrogel viscosity and was detected as an increase in the cantilever's amplitude and resonance frequency due to reduced viscous damping. This approach is sensitive but requires a power source, relatively large and complex electronics and antenna to drive the cantilever circuit and transmit the signal wirelessly.

Inspired by Ehrlich's work, we aimed to create a simple yet effective fluorescence-based sensor to detect changes in viscosity due to de-gelation activity, and monitor the

fluorescence transdermally. In place of piezoelectrically driven cantilevers, we applied an oscillating magnetic field to drive the rotation of magnetic particles (MagMOONs) embedded in the gel, and measured the ability of the MagMOONs to rotate and align with the field by detecting the modulated fluorescence signal. In general, the rotational motion of magnetic particles depends upon the applied magnetic field, the magnetic moment of the particle, shape and size-dependent drag, and the viscoelastic properties of the environment. For a given set of particles the rotational motion can be used to monitor changes in the environment. If particles are optically asymmetric, the motion can be tracked optically on a single particle level (provided that the particles can be resolved, i.e. tissue does not scatter the light). For example, in 1950, Frances Crick monitored the rotational motion of micron sized aspherical particles in response to pulsed magnetic fields to measure the viscosity in chick fibroblasts [21]. Optical tracking of rotating magnetic particles was used to monitor changes in drag during growth of single bacteria on MagMOONs [22] to monitor changes in shape of single cancer stem cells [23], to measure the viscosity of butterfly saliva [24], and to detect bacteria based on changes in viscosity when bacteria excrete biofilm polymers [25]. In addition, particle rotation has been used to track intracellular transport [26, 27]. McNaughton and colleagues used asynchronous magnetic bead rotation (AMBR)-based biosensor to measure viscosity and to detect microbial growth based upon increased drag on the magnetic particles. They applied a circularly rotating magnetic field that caused the particles to rotate at the driving frequency (with a phase delay) when the rotation was slow (and/or the field is strong), or in an asynchronous rocking motion superimposed with a continuous rotating when the rotation exceeded a critical frequency ($\omega_c = mB/\kappa\eta V$), where B is the applied field, $\kappa$ is a shape factor (6 for a sphere), $\eta$ is the viscosity, and V is the particle volume. When the viscosity of the environment surrounding the bead changed or the effective volume changed (e.g. due to a bacterium binding onto the bead surface), the rotational period of the bead changed accordingly [25, 28]. This method has high sensitivity at the single bacterium and single cell level [29]. However, the method does not work unless single particles can be resolved because each particle rotates asynchronously and no large group of particles would be aligned with each other at any given time.

Although local viscosities can be probed by optically tracking the motion of magnetically driven particles in vitro, such tracking is challenging to perform through tissue for three reasons: first, the excitation light and probe fluorescence is attenuated by the tissue; second, the tissue autofluorescence can obscure the probe signal from the probes; third, tissue scattering will cause the image to blur preventing accurate determination of the position of single particles. Fortunately, these limitations can be circumvented using MagMOONs. MagMOONs are fluorescent particles with an orientation dependent fluorescence signal generated by vapor depositing metal onto one hemisphere of a fluorescent particle and a magnetic moment that causes them to align in an external magnetic field, (**see Fig. 1** and methods section below). The MagMOONs feel a torque to align with an external magnetic field. If the MagMOONs are free to rotate in an oscillating external magnetic field, they blink as they flip between dim and bright orientations. Tissue does indeed attenuate the MagMOON fluorescence signal, but acceptable signals can be obtained by choosing the proper wavelength of the fluorescence excitation and emission as well as particle concentration. In the current study, a 50 mW 514 nm Ar ion excitation laser was found to be

sufficient to detect through 4 mm tissue thickness 400 μL MagMOONs solution 1 to $2 \times 10^4$ particles/mL (ca. 50 to 100 ng/mL, formed ~ 800 μm thick layer of solution between two 1 inch diameter coverslips). It is expected that larger depths will be attainable for higher concentrations of red or near-infrared-exciting and emitting MagMOONs. The problem of autofluorescence can be overcome because only the probe signal is modulated by the external magnetic field. This allows measurements even when the background fluorescence is thousands of times more intense than the probes and changes in time due to photobleaching and physiological changes, as long as these changes occur at different frequencies from the MagMOON modulation. Ultimately, the signal to noise ratio is limited by noise on the background at the driving frequency including shot noise on the background fluorescence [30]. Importantly, tissue scattering blurs the probe signal with a point-spread-function approximately equal to the tissue depth [31, 32] and also reduces the contrast between bright and dim MagMOON orientations as scattering scrambles the direction of excitation and emission light [33]. Although this scattering prevents single particles from being resolved and tracked in tissue, we can still measure the intensity change from an ensemble of particles that are driven to rotate and blink together. The work described here used uniform magnetic fields and had poor spatial resolution, however, in principle it is possible to improve the resolution either through endoscopy, or by restricting the region of modulation using appropriately designed magnetic fields and scanning the field across the sample (e.g. the field orientation and strength changes the most in the null region between opposing field sources. [34, 35]

In this study, we developed a MagMOON-based sensor film to detect alginate lyase protease activity based on the release of MagMOONs trapped in an alginate gel. Alginate was selected as a model system because it is a natural polysaccharide widely used in biomedical, especially in drug delivery due to its unique properties such as being biodegradable, injectable and chemically modifiable [2,4]. Monovalent alginate salts ($Na^+$, $K^+$, $NH_4^+$) are soluble in water while the divalent cations ($Ca^{2+}$, $Ba^{2+}$, $Sr^{2+}$) ionically link the alginate polymer chains together and cause gelation. Therefore, alginate gels are formed when transforming from the monovalent salt form to the divalent salt form, and the reverse reaction causes de-gelation. We used a calcium ion solution to induce the gelation of an alginate and MagMOONs mixture. The resulting MagMOON-trapped calcium alginate gel then was used as a sensor for detecting alginate lyase, the protease of alginate that cleaves the 1-4 O link between monomers of the alginate chain [36]. As the bonds are cleaved, MagMOONs are released from the gel matrix and become free to rotate. Each individual MagMOON can be tracked based on its blinking signal under the magnetic modulation. Therefore, the activity of alginate lyase is indicated via MagMOONs blinking signal. The technique we use in this study can also be applied in other biosensors and drug delivery systems based on enzyme-catalyzed breakdown of gel components.

## 2. Experimental Methods

The 4.8 μm fluorescent Nile Red carboxyl ferromagnetic particles were provided by Spherotech (Spherotech, Lake Forest, IL). The particles comprised a fluorescent polystyrene core and a shell containing ferromagnetic chromium dioxide nanorods. Modification of these particles into MagMOONs was described in previous papers [26, 37-39]. Briefly, 15

μL of 4.8 μm ferromagnetic fluorescent particles 1% w/v dispersion in water was mixed with 240 μL ethanol using a vortex mixer, deposited evenly onto six 25 mm-coverslips, and allowed to dry. A layer of aluminum was deposited onto the coverslips using an Auto 306 (BOC Edward, West Sussex UK) thermal vapor deposition system. During this process, aluminum vapor from a heated tungsten boat travels ballistically through vacuum to coat the glass coverslips as well as the top hemisphere of the fluorescent particles on the coverslip. The thickness of the aluminum layer was measured during deposition using a 6 MHz quartz crystal microbalance; deposition was stopped at 70 nm. The hemispherically coated MagMOONs were magnetized in a uniform field so that the magnetic moment of all MagMOONs pointed in the same direction (towards the coating) (see Fig. 1a-d). The particles were then removed from the coverslip and suspended in alginate solution as described below.

An air core solenoid with 24 mm hole diameter, 35 mm height, and 210 turns of 26 gauge magnet wire served as an electromagnet generating a magnetic field of ~ 0.5 mT at the centre of the microscope stage when powered with 0.25 A and 1 V. To modulate the MagMOONs, it was programed to switch the field from North-facing to South-facing every 5 s (for the gelation by calcium and de-gelation by ammonium) or 2 s (for all other experiments). This relatively long modulation time with the 0.5 mT applied field was used in order to provide enough time for all free particles to orient, especially to minimize read noise when extracting the modulated spectrum from the background. In future we will design a system with photomultiplier tubes to collect light from a larger field of view than the microscope which is expected to improve signal to noise ratios and allow more rapid detection with less read noise. Fig. 1e illustrates the working principle. In an oscillating external magnetic field, the MagMOONs appear to blink as they turn from a dim orientation, with the metal-coated side facing the objective, to the bright orientation, with the uncoated fluorescent side facing the objective. This blinking signal can be separation from un-modulated backgrounds by filtering the signal at the driving frequency [37]. Fig. 1g shows an example of two single MagMOONs rotating and blinking. About 30 s after adding $CaCl_2$ 0.2 M (75 s after the start of the experiment), the rotation stops as the gel forms. Although the gelation occurs suddenly, one MagMOON blinks one more time than the other indicating that there is some heterogeneity in the process.

Alginate lyase from *Sphingobacterium multivorum*, powder, >10,000 units/g solid was purchased from Sigma Aldrich (Sigma Aldrich, St. Louis, MO) and freshly made into 4 mg/mL solution in distilled water. $NH_4Cl$ and $CaCl_2$ were purchased from Acros Organics (Acros Organics, Morris Plains, NJ) and were made into 2 M and 0.2 M respectively. Sodium alginate was purchased from Alfa Aesar (Ward Hill, MA) and was freshly dissolved in distilled water to make 10 mg/mL solution. 20 μL of this solution was pipetted on a coverslip with freshly prepared MagMOONs after coating via aluminum vapor deposition and magnetizing (see previous paragraph). The area in the drop was scrapped either with a pipette tip following by pipetting the MagMOONs-alginate mixture and disperse in sodium alginate 10 mg/mL with the ratio of 70 μL sodium alginate 10 mg/mL per coverslip, or a camel hair #0 paintbrush following by sonication of the paintbrush in sodium alginate. 10 μL of the MagMOONs – sodium alginate mixture was then spread onto a 25 mm-coverslip that

was previously cleaned by plasma-etching (Harrick Plasma, Ithaca, NY) and 20 μL $CaCl_2$ 0.2 M was dropped on top of the mixture to form a ~ 100 μm thick calcium alginate gel with MagMOONs. The gel was left for 5 minutes before gently washing with distilled water. The coverslip was then left dry under ambient conditions for 30 minutes before imaging. The particle concentration in the formed gel was estimated to be ~ $5 \times 10^4$ particles/mL. To determine whether the MagMOON concentration within the film was uniform, we counted the number of particles in several images of a thin film gel made between two cover slips (0.35 mm in thickness and 15 mm in diameter) between two coverslips. We examined 36 fields of view (690 μm × 517 μm each) and counted 63 ± 17 particles per field view. The standard deviation is approximately twice what we expected from Poisson statistics, indicating that although the distribution appears random within an image, there is some heterogeneity in concentration across the film. **Fig. A.1** in the Supplementary data shows a representative image of particle distribution in a field view.

Figure 1f is a schematic of the microscope setup. A Leica DMI5000 epi-fluorescence microscope (Leica Microsystems, Bannockburn IL) with a 10x, 0.3 NA objective lens was used for all experiments. For single particle tracking experiments, the sample was illuminated using blue light excitation from a filtered mercury lamp and images were continuously acquired every 1 second (0.2 s exposure time) using ORCA- Flash 2.8 CMOS camera and HCImage software (Hamamatsu, Bridgewater, NJ). The fluorescent intensity was exported and analyzed using a single particle tracking script in Matlab program. For measurements through tissue, a 50 mW Ar-ion 514 nm laser was used as the excitation source. The emission signal was collected in an epi-fluorescence configuration using DNS 300 spectrometer (DeltaNu, Laramie, WY) equipped with an Andor DU420A-BV CCD camera and Andor software (Andor Technology, South Windsor CT) with an acquisition time of 0.2 s per spectrum.

For single particle tracking, custom Matlab scripts were written to extract from the acquired fluorescence movies the position and fluorescence intensity of single particles in time. The particle position was determined from the intensity centroid within a region around the particle, after applying a threshold to remove background signals. The total intensity of the tracked region was also recorded. Although all particles in view could be tracked simultaneously, to ensure comparable data, we selected for tracking only particles that were well separated (more than 2 particle diameters), and stayed in the field view and within a certain range of focus. In addition, we removed a few rare particles that didn't blink (either because they were uncoated or stuck to the glass), or had paths that crossed each other. Using these selection criteria, on average ~ 50% of the particles in view were trackable. For experiments performed through tissue, we collected the fluorescence spectra as a function of time during modulation. We then calculated the average intensity from 544 nm to 867 nm (just passed the long pass emission filter to the last pixel in the spectrum), in order to increase the signal to noise ratio for studying the blinking waveform in time.

For the experiment on de-gelation by $NH_4Cl$, the prepared coverslip with MagMOONs-trapped calcium alginate gel was put in an open on-stage chamber. 400 μL distilled water was added to the chamber, forming a ~ 1 mm thick water layer above the gel. During the acquisition, an additional 400 μL $NH_4Cl$ 2 M was added by pipette to cause de-gelation.

For the experiment on de-gelation by alginate lyase, the prepared coverslip with MagMOONs calcium alginate gel was pre-incubated in 400 μL distilled water at 37 °C for 10 min. During the acquisition, 400 μL alginate lyase 4 mg/mL was added to cleave the calcium alginate matrix.

To detect the effect of alginate lyase on calcium alginate matrix through tissue, the prepared calcium alginate thin film coverslip was placed in a chamber embedded with square slices of chicken breast (Tyson Foods Inc., Springdale AR), 2.5 × 2.5 inches, wrapped in clear plastic. The top chicken slice was about 1 cm thick while the bottom slice was varied from 1 mm to 6 mm. In the control test alginate lyase was denatured by boiling for 30 minutes. The alginate lyase was added right before placing the top tissue slice and starting the acquisition.

## 3. Results and discussion

To induce de-gelation of the calcium alginate gel, we used two approaches, as shown in **Fig. 2**. First, we added ammonium ions to the gel to compete with and replace the cross-linked calcium ions in the calcium alginate gel. Second, we applied alginate lyase to the gel to cleave the glycosidic 1 → 4 O-linkage between monomers of the alginate chain and cause gel destruction. In both cases initially trapped MagMOONs became free to rotate and blink along with the external magnetic field. We could effectively monitor the de-gelation process by tracking the position of single MagMOONs or the total intensity change under magnetic modulation.

We also demonstrated the ability to track through tissue the modulated fluorescence intensity from an ensemble of MagMOONs. The calcium alginate gel with entrapped MagMOONs was placed between two slices of chicken breast and a 514 nm laser excited the fluorescent signal from MagMOONs. The modulated signal decreased dramatically with the increase of tissue thickness but was clearly identified through up to 4 mm tissue.

### 3.1. Monitoring de-gelation by tracking individual MagMOON motion

Alginate includes mixed polymer chains of different arrangements of α-L-guluronate (G), and β-D-mannuronate (M) monomers. In sodium alginate, –COOH groups are partly replaced by –COONa [40-42]. Alginate gels form in the presence of divalent ions such as $Ca^{2+}$ and dissolve when monovalent ions such as $NH^{+}_{4}$ displace the divalent ions. The calcium alginate gel structure is maintained by the coordination of $Ca^{2+}$ with oxygen atoms in a cavity created by a pair of guluronate sequences along alginate chains. According to the literature during gelation, egg-box-liked dimers form first and then laterally associate to form egg-box multimer [43]. Unlike divalent cations, monovalent ions such as $Na^{+}$, $K^{+}$, $Li^{+}$ or $NH^{+}_{4}$ cannot serve as crosslinkers between guluronate sequences [44], hence the displacement of $Ca^{2+}$ ions by $NH^{+}_{4}$ ions destroys the gels.

In our experiment, we tracked the position and intensity of MagMOONs in a calcium alginate gel as a function of time during de-gelation. To destroy the gel structure and cause de-gelation, we added $NH_4Cl$ 1 M to calcium alginate gel to replace $Ca^{2+}$ ions. **Fig. 3a** shows the background-corrected fluorescent intensity as well as x- and y- displacements of a representative MagMOON. At the beginning when the MagMOON was fixed in the gel, its

intensity remained unchanged with time because the gel prevented it from rotating. After about 4 minutes, enough ion replacement had occurred to release the MagMOONs from the matrix and the MagMOON fluorescence began to blink in response to the oscillating magnetic field. During the de-gelation process, the amplitude of the modulation increased, presumably due to the gradually release of MagMOON from the matrix as the polymers were cleaved. We used a low magnification objective to observe many particles simultaneously, which made it difficult to accurately discern the shape of the fluorescent crescent as the MagMOON rotated. However, the shape could be discerned well enough to determine that after ~ 320 s, the MagMOON was almost fully modulated (fully bright to fully dim). To compare the de-gelation behavior of multiple particles with different volumes and fluorescence intensities, we define the “de-gel time” as the point when the modulated amplitude reached 20% the maximum amplitude. We removed from analysis particles that clearly moved out of focus before fully modulating. The de-gel time of the above MagMOON was determined to be ~ 300 s, as measured from the short-time Fourier transform spectrogram (see **Fig. A.2** in Supplementary data). Fig. 3b shows the position tracks of four individual MagMOONs in the observation view (including the representative one plotted in Fig. 3a). The initial position is marked with a black star, and the position at the de-gel time is marked with a colored dot (with the color indicating the de-gel time). Plotting the displacements and de-gel time together revealed interesting information about the heterogeneity of the de-gel process. First, it is clear that the particles followed almost the same path indicating that the entire gel flowed together in this region. Second, there was significant heterogeneity in de-gel time, with one of the four particles (yellow spot) taking twice as long to blink as the other three and moving about 20 μm before it blinked.

Having successfully tracked MagMOONs during de-gelation by ammonium ions, we next used the MagMOON-trapped calcium alginate gel to detect de-gelation from alginate lyase activity. Alginate lyase catalyzes alginate degradation by cleaving the 1-4 O linkage between monomers [36, 42]. As the chains are cleaved, MagMOONs are released and become free to rotate with the magnetic field. We pre-incubated the prepared MagMOONs calcium alginate gel coverslip in 400 μL distilled water at 37 °C for 10 minutes before acquisition. During the acquisition 400 μL alginate lyase 4 mg/mL was added to cleave the calcium alginate matrix. Fig. 3c shows the x, y-position and background-corrected intensity of a representative MagMOON immediately following 2 mg/mL alginate lyase addition. The MagMOON started to move laterally after around 350 s, as indicated by the increasing slope of × and y-displacements; however this lateral motion was not yet accompanied by fluorescence blinking. After ~600 s the MagMOON began blinking while simultaneously moving. In this case, plotting the intensity change together with the x and y-displacements elucidates the 2 steps of the de-gelation process observed. The motion during both steps was directed rather than diffusive which suggests that as the alginate gel disintegrated, convection currents were generated before particle was released and able to rotate and blink. By tracking modulation of the MagMOON intensity, MagMOON rotation was detected independently from this convective transport. The variation in de-gel time after adding alginate lyase was also presented in Fig. 3d. The color distribution indicates the de-gelation occurred from the top-left corner first then it went down on the left before spread out to the right. From Fig. 3d one can tell that all five particles have similar movement. This

observation fits well with the previous discussion on Fig. 3c about convection current and suggests that the whole gel flowed over the cover glass before the MagMOONs became free to rotate. An advantage of using MagMOONs over un-modulated probes is that MagMOON orientation could be tracked based on their blinking signal even when the gel moves.

Although these experiments tracked the intensity change from each MagMOON, all the MagMOONs responded in a similar time frame and the rotation was synchronized to the driving field, thus the average de-gelation time can also be obtained from the ensemble average intensity. In order to characterize the process of de-gelation by alginate lyase, a total of 31 particles in a field of view were tracked using our particle tracking algorithm. The algorithm calculated x, y-displacements, intensity and de-gel time (defined as 20% of maximum modulation). All the experiment parameters were the same as in Fig 3c, d. **Fig. A. 3** in Supplementary data shows the de-gel time distribution across the field view. The average de-gel time was 474 ± 18 s. Much of this variation appears co-ordinated, with shorter times on the left than the right of the view. **Fig. 4** shows that the average de-gel time determined by the average intensity of these 31 particles also agreed with that generated from the average intensity of the whole field of view.

The above tests demonstrated a simple way to detect the de-gelation process using MagMOON modulation. The MagMOONs probed both the local and overall behavior of the de-gel process. We moved a step further by testing the detection ability through different thicknesses of chicken breast. Although the position of individual particles cannot be detected through thick tissue, the total blinking signal from many particles can.

### 3.2. De-gelation tracking through tissue

Unlike conventional fluorescent dyes, untethered MagMOONs emit modulated fluorescence intensity in response to a rotating external magnetic field. This blinking property distinguishes the MagMOONs signal from the tissue autofluorescence backgrounds. To determine if the blinking MagMOON signal could be detected through tissue, we placed a film of MagMOONs in a temperature-controlled chamber between two slices of chicken breast, 1 cm thick on top and various thicknesses of 1 mm, 1.5 mm, 2.5 mm, 4 mm, and 6 mm at the bottom. During the acquisition, the temperature was maintained at 37 °C for fast and efficient enzymatic activity of alginate lyase [45]. **Fig. 5** shows the set up schematic (a) and picture (b). As mentioned in the Experimental set up section, we used a 514 nm laser at the power of ~ 50 mW as the excitation source and the emission signal was collected using a spectrometer. Although the background from tissue autofluorescence was high, the modulated probe spectrum can be revealed by subtracting the average signal in the dim orientation from the average signal in the bright orientation (see **Fig. A.4** in Supplementary data).

To ensure that only active alginate lyase caused de-gelation, a control experiment was conducted using denatured lyase. Alginate lyase was denatured by boiling for 30 minutes before adding to the gel, followed by water addition to confirm that denatured lyase did not cause MagMOON to become free to rotate. After performing these denatured lyase controls, active alginate lyase was added at 36 minutes, which indeed caused de-gelation. **Fig. 6a** shows the intensity change with time of MagMOONs through 3 mm chicken breast during

four stages of the experiment. Stage 1: During the first 7 minutes of the acquisition when calcium alginate gel was covered by a 100 μm water layer, the fluorescence from the sample (tissue containing MagMOONs) bleached quickly with no evidence of modulation. Stage 2: Throughout the 20 minutes after denatured alginate lyase addition, there wasn't a significant change except for the short term restoration of background fluorescence, likely due to small shift in tissue position directly in the laser beam, followed by approximately exponential slowdown bleaching. Stage 3: The same situation occurred after denatured alginate lyase removal and water addition. Stage 4: After addition of 2 mg/mL alginate lyase, strong MagMOON modulation was observed at the driving frequency. A short-time Fourier transform was applied to the intensity-time series to clearly present the MagMOONs modulation before and after alginate lyase addition (Fig. 6b). Stage 4 clearly shows modulation at the driving frequency of 0.25 Hz, as well as higher frequency harmonics arising from driving the modulation with a square-wave modulated magnetic field. For clarity, Fig. 6c shows the intensity of 3 represented frequencies, of which one is corresponded to the modulated frequency and two nearby frequencies (0.22 and 0.45 Hz). The strength of the 0.25 Hz frequency component is clearly higher than the background at 0.22 and 0.45 Hz.

Having successfully detected alginate lyase activity through 3 mm of chicken breast, we next studied how tissue thickness affected signal intensity. The setup was the same as shown in Fig. 5 and the results are presented in **Fig. 7**. In Fig. 7a, the fluorescent signal through 2.5 mm tissue is plotted with a smoothed curve of the original data. After subtracting with the smoothed curve to take into account for the bleaching background, the modulated and background-corrected signals through 1 mm, 1.5 mm, 2.5 mm, 4 mm and 6 mm are presented in Fig. 7b,c. Although the amplitude of modulation decreases dramatically with the increase of the tissue thickness, the modulation is clear through up to 4 mm (see the inset figure of Fig. 7c). We used short-time Fourier transform to elucidate the de-gel points (see **Fig. A.5** in Supplementary data) and obtained the values of about 5, 10, 11 and 7 minutes following lyase addition through 1 mm, 1.5 mm, 2.5 mm and 4 mm tissue, respectively. This time range agrees with the single particle tracking study where the modulation can be seen after 5 - 12 minutes (data not shown). Most of this variation is likely due to subtle differences in gel preparation. As prepared, the gel system is able to detect alginate lyase at 2 mg/mL or 60.6 μM concentration (given the molecular weight of alginate lyase is 33 kDa [45]) in 10 minutes. Figure 7d shows the signal to baseline noise ratio as a function of tissue depth, where the signal is defined as the difference between the 0.25 Hz Fourier series coefficient after de-gelation and at the start of the experiment (while the MagMOONs were still entrapped), and the baseline noise is defined as the standard deviation of the 0.25 Hz Fourier series coefficient at the start of the experiment. The signal to baseline noise ratio decreases by approximately one order of magnitude per millimeter of tissue depth; we expect it can be improved by acquiring signal over longer periods of time (e.g. using a longer window in the short time Fourier transform), using red-excited fluorophores, increasing the optical collection efficiency with a large area photodetector in place of the narrow-slit spectrometer, increasing the number of MagMOONs, or mechanically compressing the tissue). Nonetheless, the study confirmed that the MagMOON signal can be tracked through tissue to detect the presence of alginate lyase.

## 4. Conclusion

We developed a simple yet novel means to detect alginate lyase activity based upon the change in MagMOONs modulation in alginate gel before and after alginate lyase addition. The blinking MagMOON signals can be observed through tissue and separated from autofluorescence. Although we only detected through 4 mm of tissue, we used a microscope-coupled spectrometer with very small optical collection efficiency due to the small field of view and numerical aperture. In future, we plan use large area photomultiplier tubes with a lock-in amplifier for more sensitive measurements in deeper tissue. For single particle studies in situ, an endoscope will be used to collect fluorescent signals from MagMOONs through tissue. This approach can also be expanded to red-excited fluorescence, X-ray excited optical luminescence [46], and SERS [47].

## Supplementary Material

Refer to Web version on PubMed Central for supplementary material.

## Acknowledgements

This work was supported by NIH NIBIB grant, award number 1R15EB014560-01A1; the South Carolina Research Authority NSF grant 2002-593TO#0056 supported fabrication of the magnetic field control system, and a Vietnam Education Foundation (VEF) fellowship grant number F09018F to K.V.T.N. We thank Spherotech Inc. for generously donating the magnetic fluorescent particles.

## Biography

KhanhVan T. Nguyen

KhanhVan T. Nguyen got her bachelor degree in Chemical Education from Hanoi National University of Education in 2003. She had taught talented high school students for 5 years before getting a Vietnam Education Foundation fellowship and joining the Anker's Group at Clemson University, U.S.A. as a graduate student in 2009. Her research work focuses on intracellular tracking, imaging through tissue using light microscopy, and nanoparticle toxicity.

Jeffrey N. Anker, Associate Professor of Chemistry at Clemson University, received his BS in applied physics from Yale University and PhD under the supervision of Prof. Raoul Kopelman at University of Michigan. He then did a Ruth L. Kirschstein National Research Service Award NIH Postdoctoral Fellowship under the direction of Prof. Richard Van Duyne. He joined the Clemson Chemistry Department in 2008. His research involves developing imaging techniques using magnetic, plasmonic, and X-ray-excited sensors. Honors include: a grand prize at the 2002 National Inventor's Hall of Fame Collegiate Inventor's Competition, an NSRA NIH postdoctoral fellowship, and NSF CAREER award.

## References

1. Maslov MY, Edelman ER, Wei AE, Pezone MJ, Lovich MA. High concentrations of drug in target tissues following local controlled release are utilized for both drug distribution and biologic effect:

An example with epicardial inotropic drug delivery. Journal of Controlled Release. 2013; 171:201–207. [PubMed: 23872515]

2. Li Y, Rodrigues J, Tomas H. Injectable and biodegradable hydrogels: gelation, biodegradation and biomedical applications. Chemical Society Reviews. 2012; 41:2193–2221. [PubMed: 22116474]
3. Lee KY, Mooney DJ. Alginate: properties and biomedical applications. Progress in polymer science. 2012; 37:106–126. [PubMed: 22125349]
4. Tønnesen HH, Karlsen J. Alginate in drug delivery systems. Drug development and industrial pharmacy. 2002; 28:621–630. [PubMed: 12149954]
5. Brulé S, Levy M, Wilhelm C, Letourneur D, Gazeau F, et al. Doxorubicin release triggered by alginate embedded magnetic nanoheaters: a combined therapy. Advanced Materials. 2011; 23:787–790. [PubMed: 21287643]
6. Wells LA, Sheardown H. Extended release of high pI proteins from alginate microspheres via a novel encapsulation technique. European journal of pharmaceutics and biopharmaceutics. 2007; 65:329–335. [PubMed: 17156984]
7. Zhang X, Hui Z, Wan D, Huang H, Huang J, et al. Alginate microsphere filled with carbon nanotube as drug carrier. International journal of biological macromolecules. 2010; 47:389–395. [PubMed: 20600269]
8. Chang C-H, Lin Y-H, Yeh C-L, Chen Y-C, Chiou S-F, et al. Nanoparticles incorporated in pH-sensitive hydrogels as amoxicillin delivery for eradication of Helicobacter pylori. Biomacromolecules. 2009; 11:133–142. [PubMed: 19924885]
9. Queen D, Orsted H, Sanada H, Sussman G. A dressing history. International wound journal. 2004; 1:59–77. [PubMed: 16722898]
10. Rowley JA, Sun Z, Goldman D, Mooney DJ. Biomaterials to spatially regulate cell fate. Advanced Materials. 2002; 14:886–889.
11. Krebs MD, Salter E, Chen E, Sutter KA, Alsberg E. Calcium phosphate DNA nanoparticle gene delivery from alginate hydrogels induces in vivo osteogenesis. Journal of Biomedical Materials Research Part A. 2010; 92:1131–1138. [PubMed: 19322877]
12. Levenberg S, Rouwkema J, Macdonald M, Garfein ES, Kohane DS, et al. Engineering vascularized skeletal muscle tissue. Nature biotechnology. 2005; 23:879–884.
13. Thornton AJ, Alsberg E, Albertelli M, Mooney DJ. Shape-defining scaffolds for minimally invasive tissue engineering. Transplantation. 2004; 77:1798–1803. [PubMed: 15223894]
14. Gu F, Amsden B, Neufeld R. Sustained delivery of vascular endothelial growth factor with alginate beads. Journal of Controlled Release. 2004; 96:463–472. [PubMed: 15120902]
15. Ostwald W. Anomalous viscosity in mesomorphic melts. Transactions of the Faraday Society. 1933; 29:1002–1005.
16. Lapasin, R.; Pricl, S. Rheology of polysaccharide systems. Springer; 1995.
17. Bausch AR, Möller W, Sachmann E. Measurement of local viscoelasticity and forces in living cells by magnetic tweezers. Biophysical journal. 1999; 76:573–579. [PubMed: 9876170]
18. Möller W, Kreyling WG, Kohlhäufl M, Häussinger K, Heyder J. Macrophage functions measured by magnetic microparticles in vivo and in vitro. Journal of magnetism and magnetic materials. 2001; 225:218–225.
19. Ehrlich GD, Stoodley P, Kathju S, Zhao Y, McLeod BR, et al. Engineering approaches for the detection and control of orthopaedic biofilm infections. Clinical orthopaedics and related research. 2005; 59
20. Agoston A, Keplinger F, Jakoby B. Evaluation of a vibrating micromachined cantilever sensor for measuring the viscosity of complex organic liquids. Sensors and Actuators A: Physical. 2005; 123:82–86.
21. Crick FHC, Hughes AFW. The physical properties of cytoplasm: A study by means of the magnetic particle method Part I. Experimental. Experimental Cell Research. 1950; 1:37–80.
22. McNaughton BH, Agayan RR, Clarke R, Smith RG, Kopelman R. Single bacterial cell detection with nonlinear rotational frequency shifts of driven magnetic microspheres. Applied Physics Letters. 2007; 91:224105–224105.

23. Elbez R, McNaughton BH, Patel L, Pienta KJ, Kopelman R. Nanoparticle Induced Cell Magneto-Rotation: Monitoring Morphology, Stress and Drug Sensitivity of a Suspended Single Cancer Cell. PloS one. 2011; 6:e28475. [PubMed: 22180784]
24. Tokarev A, Kaufman B, Gu Y, Andrukh T, Adler PH, et al. Probing viscosity of nanoliter droplets of butterfly saliva by magnetic rotational spectroscopy. Applied Physics Letters. 2013; 102:033701–033701.
25. Sinn I, Albertson T, Kinnunen P, Breslauer DN, McNaughton BH, et al. Asynchronous Magnetic Bead Rotation Microviscometer for Rapid, Sensitive, and Label-Free Studies of Bacterial Growth and Drug Sensitivity. Analytical chemistry. 2012; 84:5250–5256. [PubMed: 22507307]
26. Behrend CJ, Anker JN, McNaughton BH, Brasuel M, Philbert MA, et al. Metal-capped Brownian and magnetically modulated optical nanoprobes (MOONs): Micromechanics in chemical and biological microenvironments. The Journal of Physical Chemistry B. 2004; 108:10408–10414.
27. Wang G, Sun W, Luo Y, Fang N. Resolving rotational motions of nano-objects in engineered environments and live cells with gold nanorods and differential interference contrast microscopy. J Am Chem Soc. 2010; 132:16417–16422. [PubMed: 21043495]
28. Kinnunen P, Sinn I, McNaughton BH, Newton DW, Burns MA, et al. Monitoring the growth and drug susceptibility of individual bacteria using asynchronous magnetic bead rotation sensors. Biosensors and Bioelectronics. 2011; 26:2751–2755. [PubMed: 21095112]
29. Elbez R, McNaughton BH, Patel L, Pienta KJ, Kopelman R. Nanoparticle induced cell magneto-rotation: monitoring morphology, stress and drug sensitivity of a suspended single cancer cell. PloS one. 2011; 6:e28475. [PubMed: 22180784]
30. Anker JN, Behrend CJ, Huang H, Kopelman R. Magnetically-modulated optical nanoprobes (MagMOONs) and systems. Journal of magnetism and magnetic materials. 2005; 293:655–662.
31. Shimizu K, Tochio K, Kato Y. Improvement of transcutaneous fluorescent images with a depth-dependent point-spread function. Applied optics. 2005; 44:2154–2161. [PubMed: 15835361]
32. Ntziachristos V. Going deeper than microscopy: the optical imaging frontier in biology. Nature methods. 2010; 7:603–614. [PubMed: 20676081]
33. Yang Z, Nguyen KVT, Chen H, Anker JN. Magnetically modulated fluorescent probes in turbid media. J arXiv preprint arXiv. 2010:1007.2863.
34. Yang N, Cohen AE. Optical imaging through scattering media via magnetically modulated fluorescence. Optics express. 2010; 18:25461–25467. [PubMed: 21164893]
35. Haegele J, Biederer S, Wojtczyk H, Gräser M, Knopp T, et al. Toward cardiovascular interventions guided by magnetic particle imaging: First instrument characterization. Magnetic Resonance in Medicine. 2013; 69:1761–1767. [PubMed: 22829518]
36. Wong TY, Preston LA, Schiller NL. Alginate lyase: review of major sources and enzyme characteristics, structure-function analysis, biological roles, and applications. Annual Reviews in Microbiology. 2000; 54:289–340.
37. Anker JN, Kopelman R. Magnetically modulated optical nanoprobes. Applied physics letters. 2003; 82:1102.
38. Behrend CJ, Anker JN, Kopelman R. Brownian modulated optical nanoprobes. Applied physics letters. 2004; 84:154.
39. Behrend CJ, Anker JN, McNaughton BH, Kopelman R. Microrheology with modulated optical nanoprobes (MOONs). Journal of magnetism and magnetic materials. 2005; 293:663–670.
40. Gacesa P. Alginates. Carbohydrate polymers. 1988; 8:161–182.
41. Grasdalen H. High-field, $^{1}$H NMR spectroscopy of alginate: sequential structure and linkage conformations. Carbohydrate Research. 1983; 118:255–260.
42. Haug A, Larsen BJ, Smidsrod O. Studies on the sequence of uronic acid residues in alginic acid. Acta Chem Scand. 1967; 21:691–704.
43. Fang Y, Al-Assaf S, Phillips GO, Nishinari K, Funami T, et al. Multiple steps and critical behaviors of the binding of calcium to alginate. The Journal of Physical Chemistry B. 2007; 111:2456–2462. [PubMed: 17305390]
44. Kevekordes K. Using light scattering measurements to study the effects of monovalent and divalent cations on alginate aggregates. Journal of experimental botany. 1996; 47:677–682.

45. Takeuchi, T.; Nibu, Y.; Murata, K.; Yoshida, S.; Kusakabe, I. Characterization of a novel alginate lyase from Flavobacterium multivolum K-11. Vol. 3. Food Science and Technology International; Tokyo: 1997. p. 388-392.

46. Chen H, Rogalski MM, Anker JN. Advances in functional X-ray imaging techniques and contrast agents. Physical Chemistry Chemical Physics. 2012; 14:13469–13486. [PubMed: 22962667]

47. Liu GL, Lu Y, Kim J, Doll JC, Lee LP. Magnetic Nanocrescents as Controllable Surface Enhanced Raman Scattering Nanoprobes for Biomolecular Imaging. Advanced Materials. 2005; 17:2683–2688.

## Highlights

- Magnetic probes with orientation -dependent fluorescence detect gelation/de-gelation.
- MagMOONs blinking signal can be observed through 4 mm chicken breast.
- MagMOONs modulation can be applied to detect protease activity.

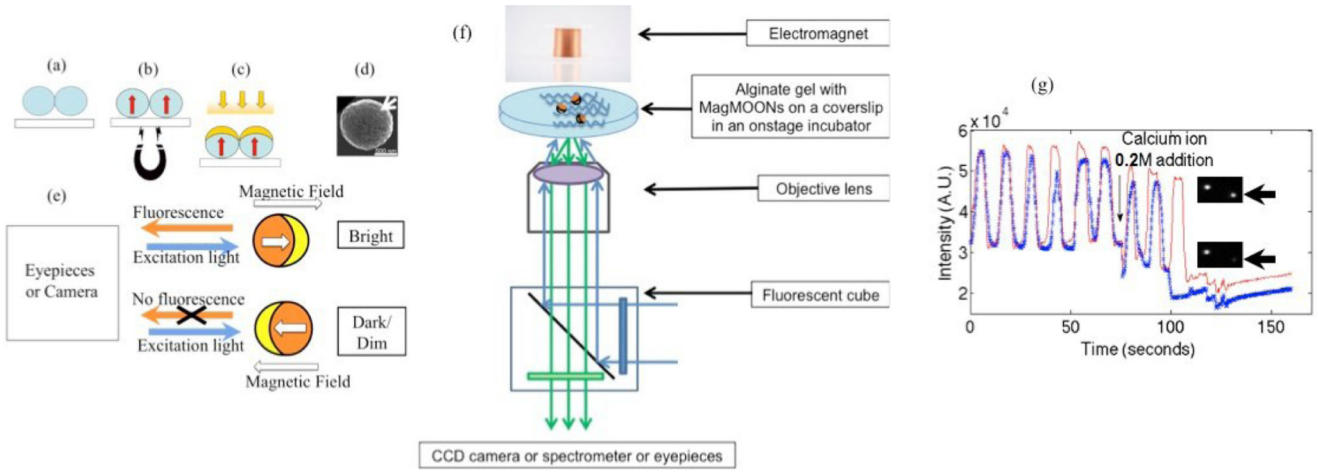


**Fig. 1.**

Principle, setup, and example of magnetically modulated fluorescence. (a)-(d) Fabrication process: (a) 4.8 μm fluorescent ferromagnetic microspheres deposited on a glass coverslip. (b) Microspheres magnetization. (c) Metal (aluminum, gold or silver) vapor deposited onto one hemisphere of the microspheres. (d) SEM image of a $Fe_3O_4$ MagMOON. The arrow points to the Au-coated side. (e) MagMOON working priciple: MagMOONs blink when they rotate in response to rotating magnetic field. (f) Schematic of fluorescence micoroscopy setup. (g) Plot of the fluorescence intensity of two single MagMOONs blinking before and after adding 400 μL $CaCl_2$ 0.2 M to 400 μL alginate 10 mg/mL (at around 75 s). MagMOONs stop blinking about 30 s after $CaCl_2$ addition, although one MagMOON (blue star) stops blinking one cycle before the other (red line). Inset shows one frame where both MagMOONs are bright, and one frame where one MagMOON is trapped in the dim orientation, while the other is still able to rotate back to the bright orientation during its last cycle.

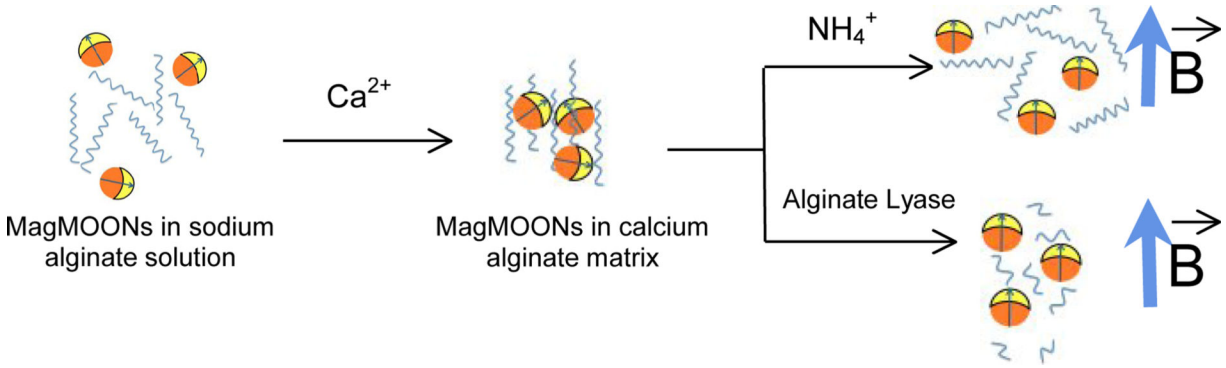


**Fig. 2.**
Summary of gelation and de-gelation experiment

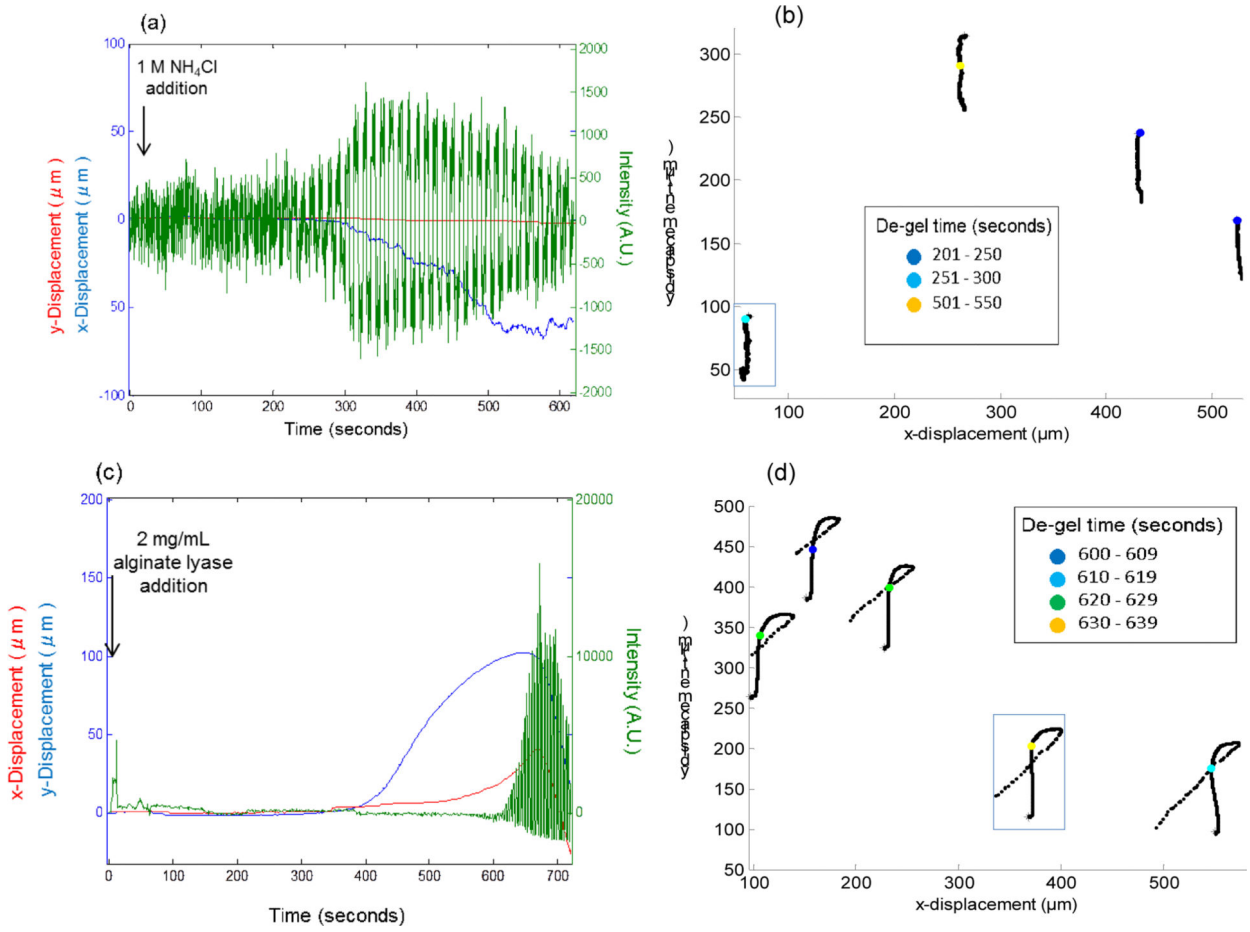


**Fig. 3.**

Tracking individual MagMOONs to detect alginate de-gelation by ammonium ion replacement (a, b) or by alginate lyase (c, d). Intensity and x, y-displacements of one representative MagMOON are plotted in (a -ammonium) and (c -alginate lyase): x-displacement (blue line, left y-axis); y-displacement (red line, left y-axis); and fluorescence intensity (green line, right axis). Modulation is seen after about 300 s with 1M $NH_4Cl$ and around 600 s with 2 mg/mL alginate lyase addition. Figures (b) and (d) are plots of de-gel time (color-coded spots) with x, y-displacements for single MagMOONs to show different MagMOONs in the same field view de-gelled at different time. The MagMOONs plotted in (a) (c) are marked in blue boxes in (b) (d). Black stars (*) indicate the initial MagMOON position.

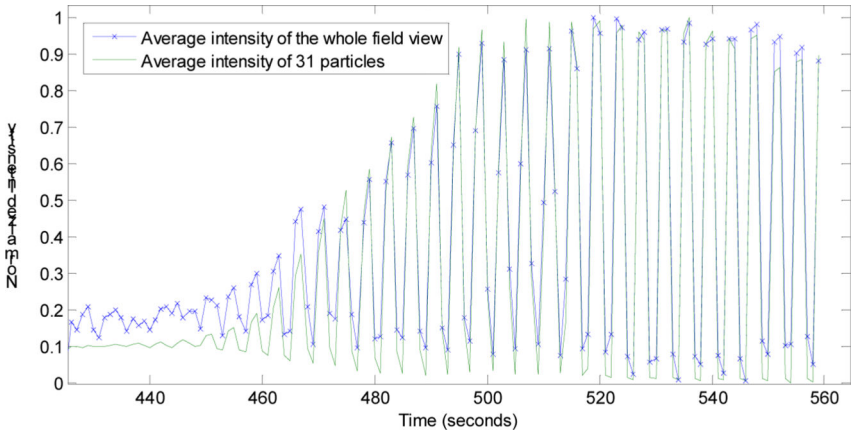


**Fig. 4.**

Plot of the average intensity of 31 MagMOONs (green line) and average intensity of the whole field view (blue star line). The intensities were normalized to aid comparison. The de-gel time determined by the average intensity of these 31 particles agrees with that generated from the average intensity of the whole field view.

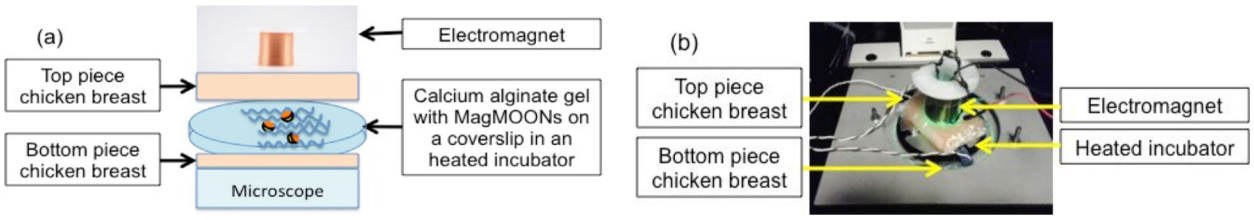


**Fig. 5.**

Fluorescent imaging through turbid chicken breast tissue. (a) Schematic of the set up for magnetic modulation and imaging through tissue. The MagMOONs are trapped in alginate calcium gel on a coverslip in an on-stage incubator chamber. This chamber is embedded in the chicken breast tissue. An electromagnet was used to modulate the MagMOONs. (b) Photo of the experimental setup.

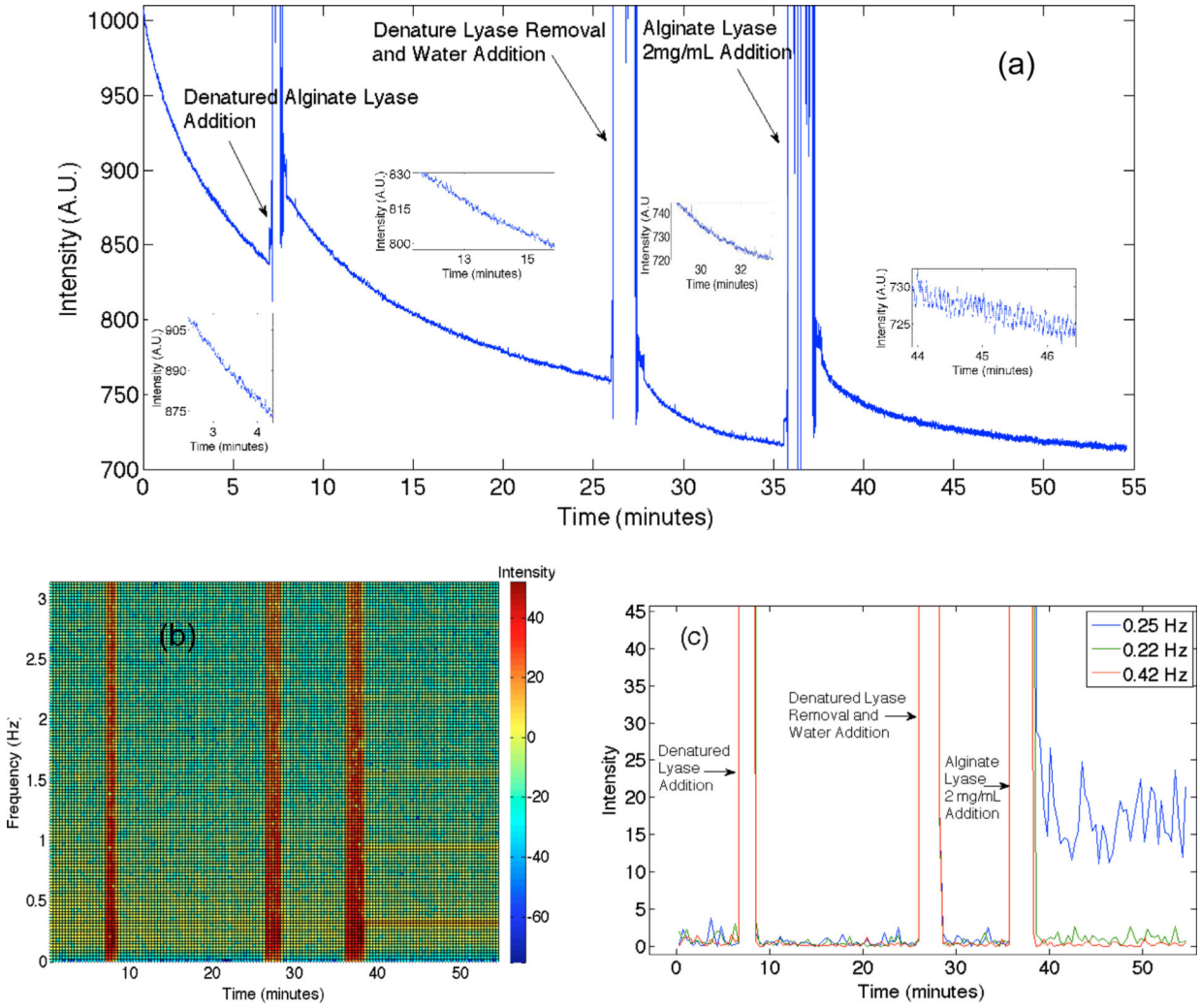


**Fig. 6.**

Monitoring of MagMOON modulation through tissue after adding denatured and active alginate lyase to the alginate gel. a) Magnetically modulated fluorescence signal through 3 mm of chicken breast using 514 nm green excitation laser during 4 stages: Stage 1: alginate gel in water; Stage 2: after adding denatured alginate lyase; Stage 3: after denatured alginate lyase removal and water addition; Stage 4: after 2 mg/mL alginate lyase addition. Modulation can be seen during Stage 4. Inset figures are zoom-ins to show modulation if present. b, c) Short-Time Fourier Transform spectrogram shows modulation after alginate lyase addition but not after addition of water or denatured alginate lyase.

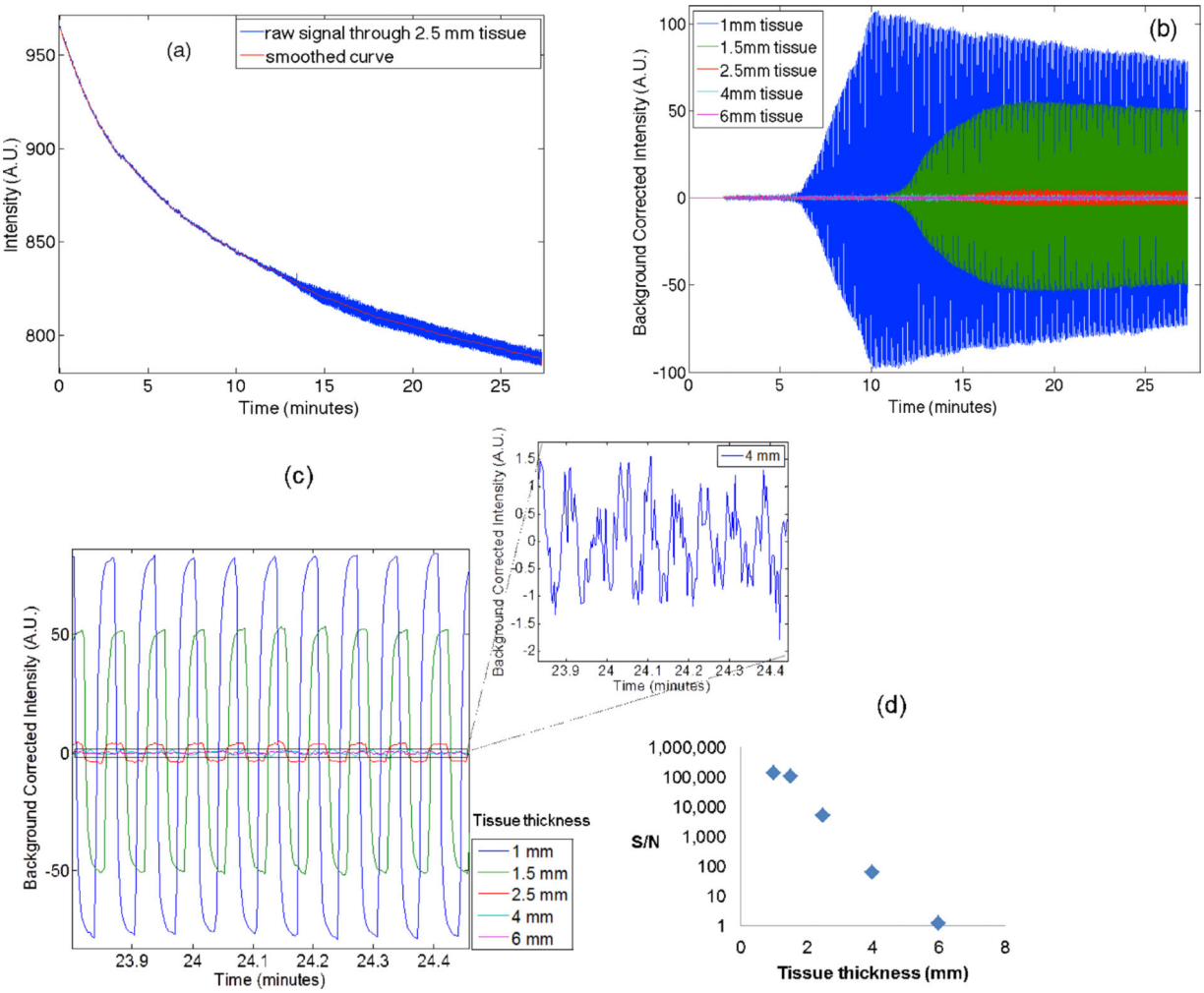


**Fig. 7.**

Detection through tissue of the de-gelation by alginate lyase. (a) Plot of fluorescence signal through 2.5 mm chicken breast and its smoothed curve. (b) Background-corrected magnetically modulated fluorescence signal through 1 mm, 1.5 mm, 2.5 mm, 4 mm and 6 mm chicken breast. (c) Zoom-in of (b) to visualize modulation. The inset figure is a more zoomed-in of the 4 mm tissue thickness case for clarity. (d) Signal to baseline noise ratio for MagMOONs viewed through different tissue thicknesses, based upon Fourier analysis (Fig. A.5).